Accepted Manuscript

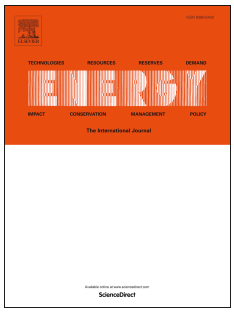

Effect of Pt loading and catalyst type on the pore structure of porous electrodes in polymer electrolyte membrane (PEM) fuel cells

Jian Zhao, Adnan Ozden, Samaneh Shahgaldi, Ibrahim E. Alaefour, Xianguo Li, Feridun Hamdullahpur

PII: S0360-5442(18)30368-2

DOI: 10.1016/j.energy.2018.02.134

Reference: EGY 12434

To appear in: *Energy*

Received Date: 21 December 2017

Revised Date: 22 February 2018

Accepted Date: 23 February 2018

Please cite this article as: Zhao J, Ozden A, Shahgaldi S, Alaefour IE, Li X, Hamdullahpur F, Effect of Pt loading and catalyst type on the pore structure of porous electrodes in polymer electrolyte membrane (PEM) fuel cells, *Energy* (2018), doi: 10.1016/j.energy.2018.02.134.

Effect of Pt Loading and Catalyst Type on the Pore Structure of Porous Electrodes in Polymer Electrolyte Membrane (PEM) Fuel Cells

Jian Zhao[a,b], Adnan Ozden[a,b], Samaneh Shahgaldi[b], Ibrahim E. Alaefour[b], Xianguo Li[a,b], Feridun Hamdullahpur[a]

[a]*Department of Mechanical and Mechatronics Engineering, University of Waterloo, 200 University Avenue West, Waterloo, ON N2L 3G1, Canada*

[b]*20/20 Laboratory for Fuel Cell and Green Energy RD&D, Department of Mechanical and Mechatronics Engineering, University of Waterloo, 200 University Avenue West, Waterloo, ON N2L 3G1, Canada*

Abstract

Catalyst layer (CL) has a significant impact on the overall pore structure of the entire electrodes, thereby impacting the transport processes and the performance of polymer electrolyte membrane (PEM) fuel cells. In this study, the contribution of the CL to the entire electrode structure is experimentally investigated. The electrodes are prepared by using two types of catalysts with different platinum/carbon (Pt/C) ratios and Pt loadings and characterized by the method of standard porosimetry (MSP). The results show that for the same type of catalysts, as the Pt loading is increased, both the porosity and mean pore size of the electrode decrease, whereas the pore surface area increases. For a constant Pt loading, a lower Pt/C ratio results in a thicker electrode with a smaller porosity, smaller pore size, and larger pore surface area. The fractal dimension is found to be a good representative of the complexity of the pore structure of the electrode; a larger fractal dimension is detected for a higher Pt loading and a smaller Pt/C ratio.

Keywords: Polymer electrolyte membrane fuel cell; Catalyst layer; Pore size; Pore surface area; Fractal dimension

1. Introduction

Polymer electrolyte membrane (PEM) fuel cell is a clean power generator suitable for a wide range of practical applications [1–8]. It has a multi-layered structure with its core component, referred to as a membrane-electrode assembly (MEA), having a proton-conducting membrane layer sandwiched between an anode and a cathode electrode; and each electrode consists of a gas diffusion layer (GDL) and a catalyst layer (CL) [9–11]. In cell operation, hydrogen and air are transported through the pore regions of the anode and cathode GDLs to the reaction sites within the CLs for electrochemical reactions and power generation [12–14]. The structure of the electrode dictates the transport processes, and hence the performance of PEM fuel cells. The importance of the GDL on the overall pore structure of the electrode is well recognized and extensively investigated [15,16], while the contribution of the CL is not.

A typical CL employed in PEM fuel cells contains electrochemically active and electrically conductive platinum (Pt) nanoparticles supported on relatively larger carbon particles, and these Pt/C particles are held together by an ionomer binder [17–19]. The morphological, microstructural and electrochemical characteristics of the CL are closely linked to its materials and design parameters, such as Pt/C ratio, Pt loading, and ionomer weight ratio. Since the CL is typically very thin, only a few micrometer thick, hence mechanically weak, it is usually deposited onto the membrane or GDL which is typically a carbon paper. The carbon paper is comprised of carbon fibers and generally has a thickness of 100-300 μm. By its very nature, the carbon paper has solid and void regions. The solid region serves as a “bridge” for electron transport, while the void region provides pathways for mass transport. The microstructural characteristics of the carbon paper depend to a large extent on the orientation of the fibers and numbers of layers stacked. The pore structure of the carbon paper is usually modified to achieve

desirable wettability characteristics – a process termed as “hydrophobic treatment”, in which the surface of the carbon paper is treated by hydrophobic agents, such as polytetrafluoroethylene (PTFE), polyvinylidene fluoride (PVDF), and fluorinated ethylene propylene (FEP). In addition, specifically for the cathode side, the micro-porous layer (MPL), composed of carbon particles and a hydrophobic agent, is deposited onto the carbon paper to achieve effective water management and interfacial transport characteristics [20]. The combination of the carbon paper and MPL is often referred to as the double-layer or dual-layer GDL.

The mass transport in both the GDLs and CLs occurs under the combined influence of relatively dominant diffusion and a lesser degree of convection [14]. The effectiveness of diffusion and convection through both the GDL and CL is represented by the effective diffusion coefficient (EDC) and permeability, which are the strong functions of the microstructural characteristics of the electrodes [21–24]. Therefore, it is of significance to understand the pore structure of the entire electrode (GDL+CL).

The microstructural characteristics of the porous electrodes are quantitatively represented by the terms of “porosity” and “pore-size distribution” [25]. The porosity is the ratio of the pore volume over the bulk volume, while the pore-size distribution provides information about the distribution of the pore volume or area with respect to pore size. The pore volume represents the volume of the void region including open and closed pores, while the bulk volume is the cumulative volume of solid and void regions. However, many engineering problems require more comprehensive information that cannot be fully obtained by determining these two parameters – this makes the identification of other parameters, such as bulk density, mean pore size, and pore surface area, essential [25]. The bulk density is defined as the ratio between the mass of the porous sample and the bulk volume. The mean pore size is the strong function of the shapes of the pores, and it can

only be precisely determined when the shapes of the pores are known. However, most pores in the electrodes are of irregular shapes. Thus, the mean pore size of the electrodes generally relies on the assumption that the shape of the pores is constant and cylindrical [26]. More recently, the functionality of another parameter termed as "fractal dimension" has also been greatly appreciated [27–29], specifically for investigating the capability of the porous media for mass transport (see [27,30–39], for example). The fractal dimension is a measure of the complexity of the porous media, and it can take non-integer values between 2 and 3, depending on the complexity of the fractal surface – the more it approaches to 3, the more complex the surface is [37,40,41].

As mentioned earlier, optimization of the electrodes requires a comprehensive understanding of the structure of the entire electrode (GDL+CL). However, thus far, the focus of the studies on microstructural characterization has been mainly centering upon investigating the pore structure of the carbon papers and double-layer GDLs (see [15,42–45], for example), with few studies directed towards the entire electrode (GDL+CL). The available studies have significantly contributed to the literature by revealing the influence of the pore structure of the GDL on various phenomena, i.e., the transport of mass, heat, and electricity – this has enabled the manufacture of fuel cells that can operate at high-current densities, which is fairly desirable for practical applications [46]. However, optimization of the electrodes for optimum performance, durability, and stability requires a complete understanding of the entire pore structure. It is thus critical to understand exactly what type of pore structure is achieved upon deposition of the CL, or how the CL design parameters, i.e., catalyst type and catalyst loading, influence the pore structure of the electrode. It might be mentioned that Yu et al. [47] investigated the pore size distribution of the catalyst layers deposited on the reference ethylene tetrafluoroethylene (ETFE)

substrate and the results are compared with the reference ETFE substrate. Their studies investigated the changes in pore size distribution with a focus on the ionomer/carbon ratio of the catalyst layer.

The objective of the present study is therefore to address these open questions by characterizing the catalyzed electrodes (GDL+CL) with different specifications in terms of porosity, pore size distribution, pore surface area, mean pore size, and fractal dimension. The catalyzed electrodes are prepared by using two types of catalysts (i.e., 30% and 60% Pt/C particles) with Pt loadings of 0.1 and 0.4 $mg \cdot cm^{-2}$. Comparison is made with an uncatalyzed electrode, or GDL only. The MSP is selected to characterize the pore structures of the electrodes, owing to its capability of measuring a wide range of pore size under room conditions without damaging the pore structure of the electrode [48]. The electrode characteristics measured in this study will be useful for the analysis and simulation of the transport phenomena in the electrode and cell performance.

2. Experimental

2.1. Electrode Preparation

The electrodes investigated in the present study are prepared by following a procedure that involves three steps. For brevity, only the procedure followed for the electrode made of carbon supported platinum (Pt/C, 30 wt.%) with the Pt loading of 0.4 $mg \cdot cm^{-2}$ is described. The first step is the preparation of the catalyst ink, through which the commercially available carbon-supported platinum (Pt/C, 30 wt.%), 5 wt.% Nafion® solution, deionized (DI) water, and isopropyl alcohol (IPA, 99.9%, Sigma-Aldrich®) are consecutively mixed in a vial and then ultrasonically blended for 1 h to achieve a uniform suspension. The weight ratio of the catalyst to Nafion® in the ink is set at 3:1. The resulting slurry is spray-deposited onto the MPL surface of

the commercially available PTFE-treated GDL (Avcarb GDS3250) until the catalyst loading of 0.4 $mg \cdot cm^{-2}$ is achieved. Lastly, the catalyzed electrodes are dried at 60°C for 2 h to evaporate any remaining moisture. In this study, five types of samples are tested in order to investigate the effect of Pt loading and catalyst type on the pore structure of the electrodes. These five types of the samples include an uncatalyzed GDL, and four catalyzed GDLs made of 30 and 60% Pt/C with 0.1 and 0.4 $mg \cdot cm^{-2}$ Pt loading, respectively.

2.2. Method of Standard Porosimetry (MSP)

2.2.1. Experimental Setup

The pore structures of the electrodes under investigation are determined by the method of standard porosimetry (MSP) [49–51], owing to its advantages, such as it is a non-destructive method and has a capability of detecting the pores located in a broad range (0.3 nm-300 μm) under room conditions. The experimental setup for the pore characterization of the electrodes is equipped with the following constituents: a heating bottle, a vacuum pump, aluminum clamping devices, a digital balance, a manipulating robot arm, and a drying station. The heating bottle is used to remove the moisture from the samples prior to measurements, while the vacuum pump is employed to provide a vacuum environment during the drying step to ensure that the pores in the porous media are free of moisture in the air. The aluminum clamping devices are used to keep the samples stacked in a fixed position. The digital balance with high accuracy is utilized to measure the change in the weights of the stacked samples over time. The manipulating robot compatible with commercial software is used to move the samples between the digital balance and drying station at certain time intervals. The drying station is the place where the samples are kept at a constant temperature of about 45°C to speed up the evaporation of the working fluid. In

the measurements, octane is chosen as the working fluid, due to its advanced wetting characteristics.

2.2.2. Experimental Procedure

The MSP utilizes the capillary pressure equilibrium between the bodies in contact to determine the capillary pressure curve of the sample under test. This method employs three samples: two of them are standard with known pore size distribution, and the other is the sample extracted from the test of interest electrode. Prior to measurements, two pieces of disk-like samples (23 mm in diameter) are extracted via a die. The two layers of test samples (each of them is about 220-230 μm thick) are situated together as an individual test object – that is, the test sample is thick enough to contain sufficient amount of octane, enabling us to obtain measurements from an adequate number of measurement points. Thereafter, the test and standard samples are situated in a glass tube and drained at 180°C for 1 h under a vacuum environment to remove any moisture. Subsequently, the test sample, along with the two standard samples, is soaked in octane at room temperature under a vacuum environment for 10 min to ensure that the pores of the samples are completely filled with octane. On completion of octane immersing process, the samples are taken out of the beaker, and excess octane is gently wiped off from the sample surfaces. The test sample is sandwiched between the standard samples via clamping devices; and in this case, it is known that the test sample is in capillary equilibrium with the standard ones. Also, any variation from the capillary equilibrium due to evaporation will affect both the test and standard samples, allowing determination of the capillary curve of the sample under test from the known capillary pressure curves of the standard samples. Thus, the change in the weight of the samples due to evaporation is periodically measured by moving the clamping devices at 3-min time intervals between the drying station and digital balance. During each measurement, the clamping devices

are separated individually, and the mass of each clamping device (upper, middle, and lower) with the corresponding test sample is recorded. Therefore, the mass of the octane evaporated from the samples can be calculated by the weight difference between the two consecutive measurements. This provides a precise determination of the volume of the remaining octane occupying the pores at the corresponding time intervals. The variation in the samples weights is recorded until the samples are completely dried – this corresponds to ~100 consecutive measurements. The last step is establishing the correlation between the pore volume and pore radius of the test sample by utilizing the capillary pressure curves of the standard samples.

2.2.3. Data Analysis

The method of standard porosimetry (MSP) is developed based on the laws of capillary equilibrium [49–51], which states that if two or more porous materials stay together for a sufficiently long time in a wetting liquid, they will have the same capillary potentials (capillary pressure is a kind of capillary potential):

$$p_{c_1} = p_{c_2} = p_{c_i} = p_c \tag{1}$$

where p_c is the capillary potential of i^{th} layer.

The MSP experimentally determines the relationship between the liquid volume (V_t) in the test sample and the liquid volume (V_s) in the standard sample:

$$V_t = f_V(V_s) \tag{2}$$

The liquid distribution in the standard sample can be expressed as a function of p_c and is provided by the manufacturer as follows.

$$V_s = f_s(p_c) \tag{3}$$

The liquid distribution in the tested samples regarding p_c is determined:

$$V_t = f_V[f_s(p_c)] \tag{4}$$

The capillary pressure (or capillary potential), p_c, can be expressed as the Young-Laplace equation [49]:

$$p_c = -\frac{2\sigma\cos\theta}{r_m} \tag{5}$$

where σ is the surface tension of the liquid, θ is the wetting angle, and r_m is the maximum pore radius filled with liquid. Here, the value of p_c is one of the capillary potentials, hence the function between V_t and r_m becomes:

$$V_t = f_V\left[f_s\left(-\frac{2\sigma\cos\theta}{r_m}\right)\right] = F(\theta, r_m) \tag{6}$$

For octane, the wetting angle is almost zero for all materials, thus Eq. (6) is simplified to,

$$V_t = f_V\left[f_s\left(-\frac{2\sigma}{r_m}\right)\right] = F(r_m) \tag{7}$$

On the other hand, the total pore volume, V_p, of the test samples can be determined as follows:

$$V_p = \frac{m_{sat} - m_{dry}}{\rho} \tag{8}$$

where m_{sat} is the total mass of the saturated sample, m_{dry} is the total mass of the dry sample, and ρ is the density of the octane.

Then the bulk volume, V_b, can be calculated:

$$V_b = \frac{\pi d^2 \delta N}{4} \tag{9}$$

where d is the diameter of the test sample, δ is the thickness of the sample and N is the number of the samples being tested together. In this case, d = 23 mm, and N = 2.

The porosity, $\emptyset$, is defined as:

$$\emptyset = \frac{V_p}{V_b} \tag{10}$$

The pore surface area, S_p, can be calculated from the integral pore radius distribution curve by using the following equation [48]:

$$S_p = 2 \int_{r_{max}}^{r_{min}} \frac{1}{r} \frac{dV_t}{dr} dr \tag{11}$$

The specific surface area, SSA, is defined by the following equation in order to make a good comparison with other samples,

$$SSA = \frac{S_p}{V_b} \tag{12}$$

The mean pore size, MPS, is defined as [26]:

$$MPS = \frac{4V_p}{S_p} \tag{13}$$

The fractal dimension, D, can be determined based on the relation between the fractal surface area, S_p, and the pore radius or "scale", r, used to measure the surface area, according to the following relation,

$$SSA = kr^{2-D} \tag{14}$$

where k is the constant that describes the shape of the solid elements in the porous media. The values of k and D can be determined by curve fitting of the pore surface area distribution using Eq. (14).

3. Results and Discussion

The pore structures of the prepared electrodes are investigated by the method of standard porosimetry (MSP) in terms of pore size distribution (PSD), porosity, pore surface area distribution, specific surface area (SSA), and mean pore size (MPS), and surface fractal dimension.

3.1 Pore Size Distribution

Pore size distribution is the relative amount of each pore size in a representative volume of porous materials [52] and is usually represented by a probability density function indicating the pore volume at a given pore size. Since the pore shapes in natural objects are mostly irregular, the pore size is only meaningful when the equivalent pore shapes are assumed. In most porous media, the pore sizes are distributed over a wide range of values, and this parameter quantitatively describes the uniformity and complexity of the pore structure.

Fig. 1 (a) and (b) indicate the cumulative pore size distribution of the electrodes containing two different types of catalyst with the Pt/C ratios of 30% and 60%, respectively. As can be seen, for

the low Pt loading of 0.1 mg·cm^{-2}, the volume of the pores larger than 1 μm is decreased slightly for both two types of catalysts in comparison with the uncatalyzed GDL. This is likely due to the penetration of the small catalyst particles and ionomers into the GDLs; therefore, some large pores are occupied by the catalyst particles and ionomer, leading to a slight decrease in the volume of large pores. However, as the Pt loading is increased to 0.4 mg·cm^{-2}, these two types of catalysts behave differently. For 30% Pt/C, the large pores (>1 μm) continue to reduce since the catalysts and ionomers trend to penetrate into and occupy more large pores; while for 60% Pt/C, more large pores are introduced by the thicker catalyst layers. In other words, the pore volume and pore size distribution of the electrodes can be changed by two means: reduced pore volume due to the material (catalyst particle and ionomer) penetration into GDLs and increased pore volume due to the presence of the deposited catalyst layers. The combined effect of these two factors should be further determined based on other parameters, e.g., porosity.

Fig. 1 (c) and (d) exhibit the differential pore size distribution of the electrodes with two different types of catalyst, 30% and 60% Pt/C, respectively. The radii of the pores can be as large as 10 μm. It is seen that for the same type of catalyst, as the Pt loading is increased, the volume of the pores smaller than 100 nm increases (also see Fig. 1 (a) and (b)). This increase is likely due to the presence of more catalyst particles in the CLs with higher Pt loadings. For the constant Pt loading, the volume of pores smaller than 100 nm for 30% Pt/C (see Fig. 1 (a)) is much higher than that for 60% Pt/C (see Fig. 1 (b)). This implies that a lower Pt/C ratio requires more carbon particles in order to maintain the same Pt loading, and a larger amount of carbon particles leads to a significant increase in small pores, formed between the carbon particles with a diameter range from 30 to 50 nm.

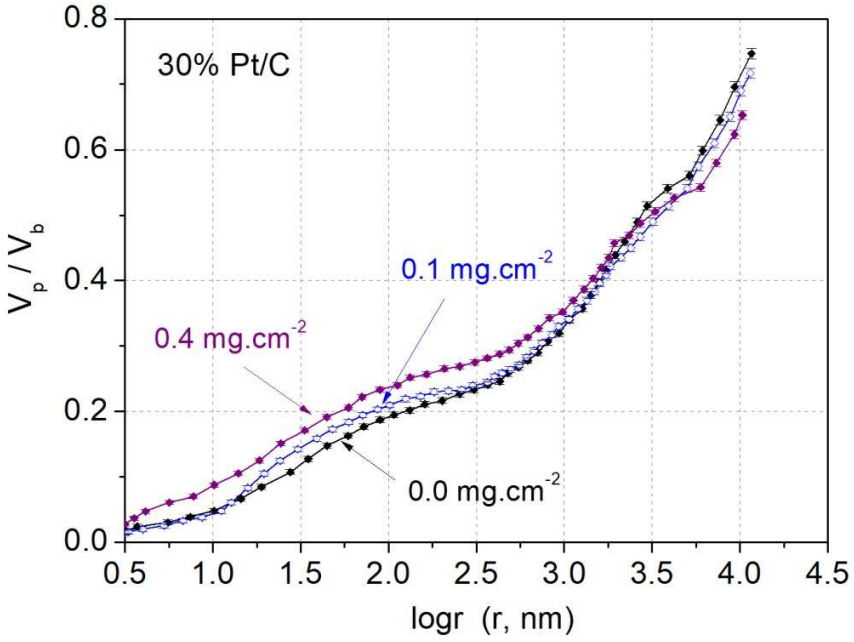

(a) Cumulative pore size distribution for 30% Pt/C.

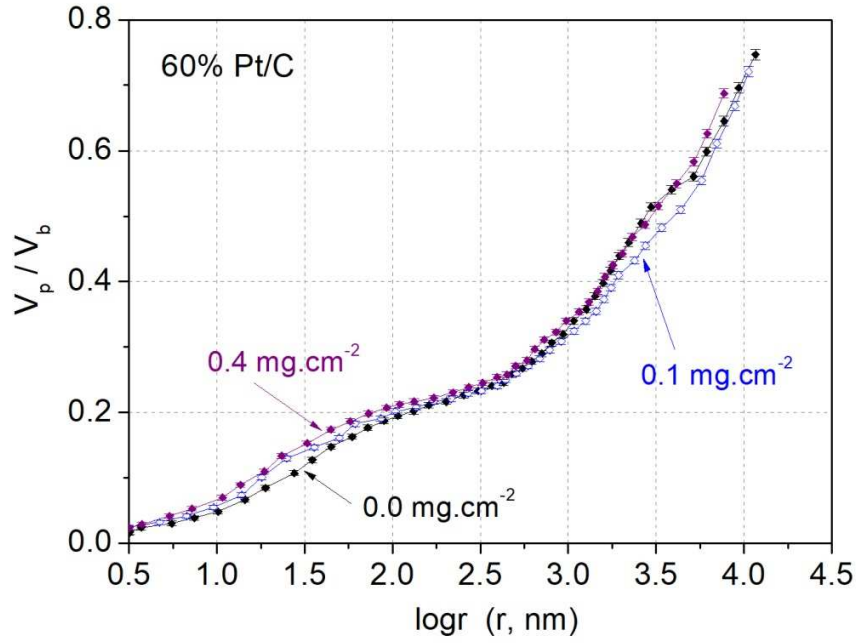

(b) Cumulative pore size distribution for 60% Pt/C.

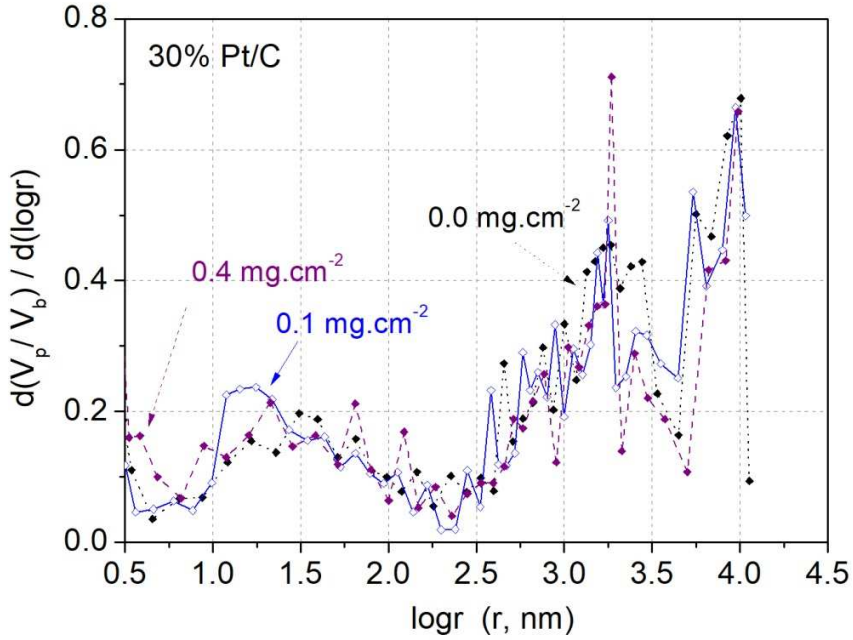

(c) Differential pore size distribution for 30% Pt/C.

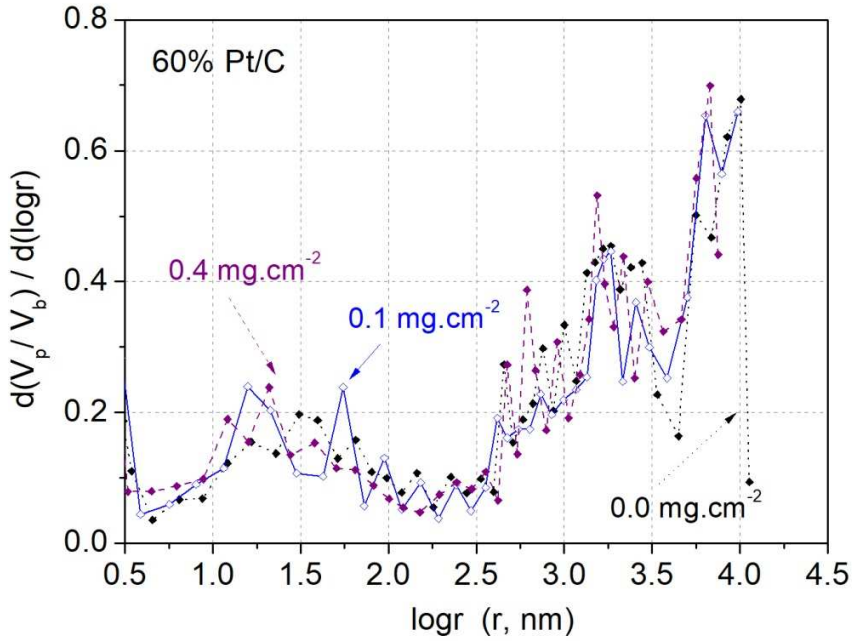

(d) Differential pore size distribution for 60% Pt/C.

Fig. 1. Pore size distribution (PSD) of the porous electrodes with the Pt loadings and catalyst types of (a) cumulative PSD for 30% Pt/C, (b) cumulative PSD for 60% Pt/C, (c) differential PSD for 30% Pt/C, and (d) differential PSD for 60% Pt/C, (V_p is pore volume, V_b is bulk volume, and r is the pore radius.)

3.2 Porosity

Porosity is a measure of the volumetric fraction of the pores in a porous medium. A larger porosity indicates that there are more void regions in the porous media which can be used for transporting oxygen, hydrogen, and water in PEM fuel cells, yielding a smaller mass transport resistance, hence a better cell performance. Therefore, to accurately measure the porosity is of great significance for the performance of the electrodes as well as the PEM fuel cells.

Fig. 2 (a) and (b) present the relationships between the pore volume, bulk volume, and porosity for the electrodes with the two types of catalysts (30% and 60% Pt/C) studied, respectively. It can be observed that for a given type of Pt/C catalyst, the bulk volume presents a linear increase with the Pt loading since the amount of CL ingredients (Pt/C and ionomer) increases proportionally. This is because for a given type of Pt/C catalyst, an increase in the Pt loading increases the thickness of the electrode, since the cross sectional area of the sample is fixed. For example, the electrode thickness increases from 221.6±2.1 μm to 243.0±2.1 μm for 30% Pt/C and to 231.0±2.1 μm for 60% Pt/C, respectively [53], as calculated based on Eq. (9) with the given bulk volumes as shown in Fig. 2. However, the pore volume of these electrodes does not change too much. As the porosity is defined as the ratio of pore volume to bulk volume, the porosity of the electrode for a higher Pt loading is decreased significantly. Similarly, for the same Pt loading, a higher Pt/C ratio requires fewer amounts of carbon and ionomer, thus

resulting in a thinner electrode with a smaller bulk volume. Therefore, a Pt/C ratio of 30% results in a thicker and less porous electrode as compared to that of 60% Pt/C.

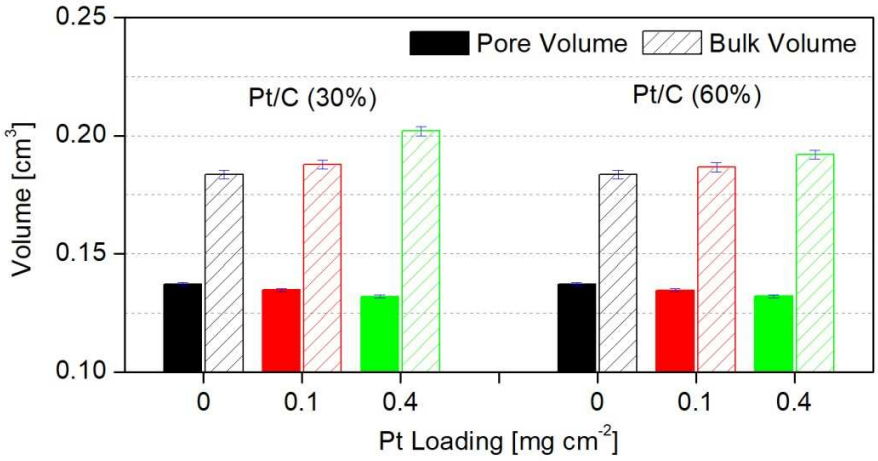

(a) Pore volume and bulk volume.

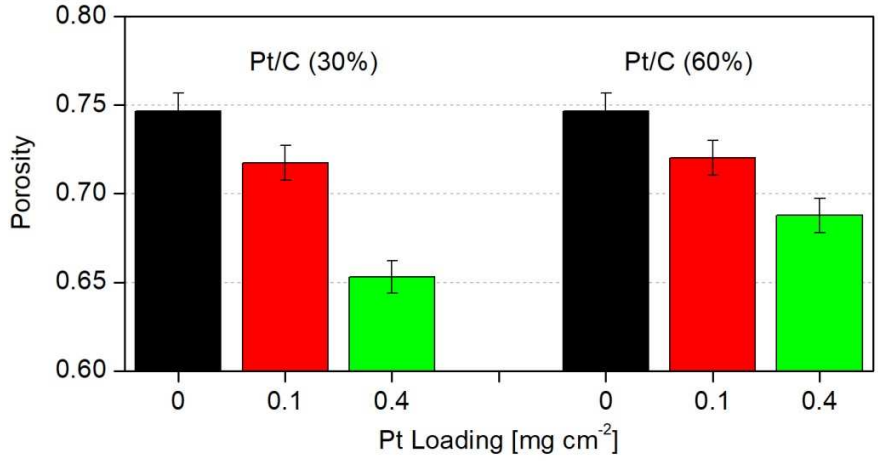

(b) Porosity.

Fig. 2. Pore volume and porosity of the electrodes with various Pt loadings and two types of catalysts of 30% and 60% Pt/C.

3.3 Pore Surface Area Distribution

Pore surface area distribution, similar to PSD, is defined in this section as the probability density function of the amount of surface area at a given pore size. This parameter quantifies the surface area in either large or small pores and can be an indicator of the amount of electrochemical reaction sites.

Fig. 3 (a) and (b) indicate the cumulative surface area distribution of the pores from the maximum to minimum size for these five types of the prepared electrodes. The cumulative surface area shown represents the total pore surface area integrated from the maximum pore sizes to the given pore size, normalized by the total bulk volume of the sample involved. As can be seen, the surface area is greatly contributed by the small pores, e.g., 95.0%-96.5% for the pores with a radius smaller than 100 nm. In addition, for 60% Pt/C, 0.1 $mg \cdot cm^{-2}$ Pt loading leads to a 1.2% increase in the specific surface area, while 0.4 $mg \cdot cm^{-2}$ Pt loading causes a 24.0% increase. The rises of the pore surface area are contributed by the presence of small Pt/C particles, resulting in more chemical reaction sites. Further, for a smaller Pt/C ratio, more surface area can be observed with a constant Pt loading. The increase in surface area is due to the larger amount of carbon particles utilized. Meanwhile, only the pores larger than 3.2 nm is considered in order to study the pore surface area. This is because the pores with a range from 0 to 3.2 nm have negligible volumes as shown in Fig. 1 (a) and (b), while the relative uncertainty in pore volume within this range can be as large as 100%. Therefore, the surface area calculated from the pores with a size range from 0 to 3.2 nm is unreliable, which is excluded in the pore surface area analysis in this study.

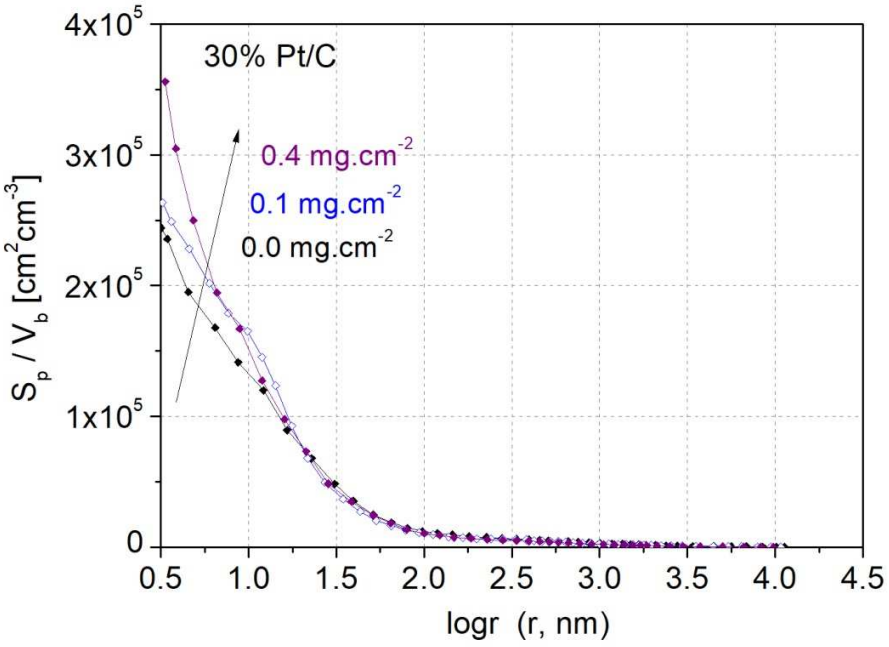

(a) Cumulative surface area distribution for 30% Pt/C.

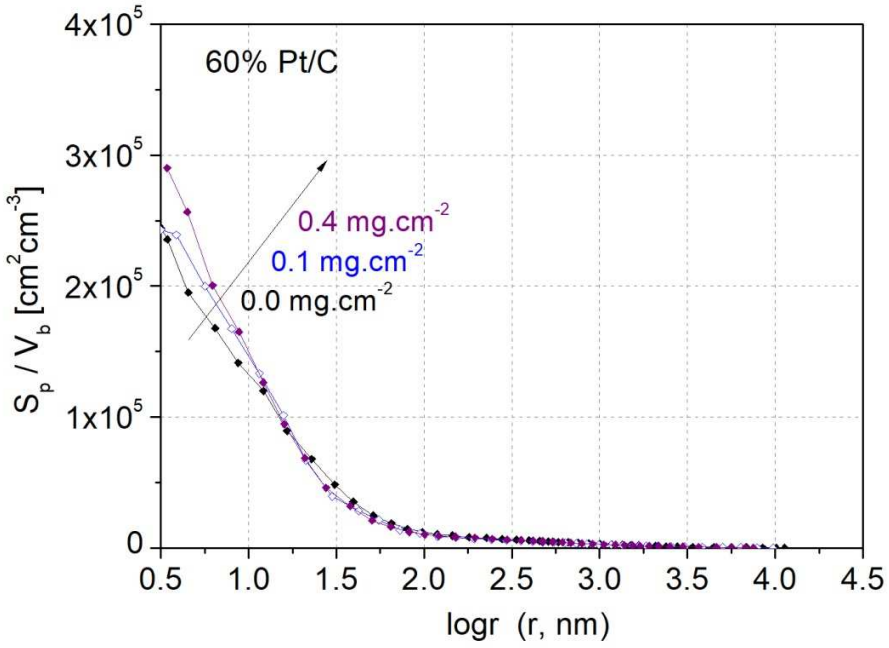

(b) Cumulative surface area distribution for 60% Pt/C.

Fig. 3. Cumulative surface area distribution of the porous electrodes with various Pt loadings and different types of catalysts: (a) 30% Pt/C and (b) 60% Pt/C.

3.4 Specific Surface Area (SSA)

Specific surface area is defined as the total surface area of a material per unit of mass or bulk volume. It has a particular importance for reaction rate, permeability, and other physical properties. Fig. 4 represents the volume-based specific surface area for the uncatalyzed and catalyzed electrodes considering the pores larger than 3.2 nm, as defined by Eq. (12) earlier. As can be seen, as more catalysts are deposited on top of GDLs, the specific surface area increases significantly. For example, for 30% Pt/C, even though the thickness of the 0.4 mg.cm^{-2} is increased by only 7.5% in comparison with that of the 0.1 mg.cm^{-2}, the specific surface area is increased by 35.2%. Similarly to the 60% Pt/C, the thickness increase is only 2.9%, while the SSA increase can be 19.4%. The increase in the surface area is contributed to by the small pores formed due to the presence of the catalyst particles.

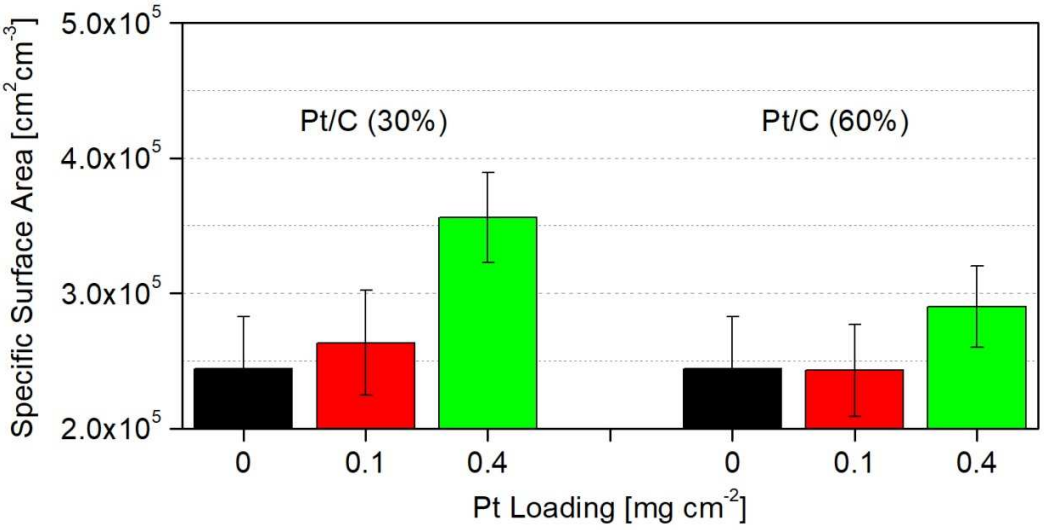

Fig. 4. Specific surface area of the porous electrodes with various Pt loadings and different types of catalysts.

3.5 Mean Pore Size

The mean pore size is defined as four times of the pore volume to the corresponding pore surface area. It represents the characteristic size of the pathways in the porous media, and a smaller mean pore size indicates that it is more difficult for reactant gases or product liquid to pass the media.

Fig. 5 presents the mean pore size of the electrodes with various Pt loadings and different types of catalysts. For the same type of catalysts, as the Pt loading is increased to 0.4 mg·cm^{-2}, more Pt/C particles and ionomers are deposited on the GDLs. Because the CL is becoming thicker, the mean pore size decreases accordingly. The mean pore size is equal to four times the ratio of pore volume to pore surface area. A slight decrease in pore volume and a significant increase in pore surface area lead to the decrease in the mean pore size. In addition, for the constant Pt loading, reducing the Pt/C ratio leads to a significant drop in mean pore size. This is expected because a small Pt/C ratio results in more small pores in the electrode as discussed in previous sections.

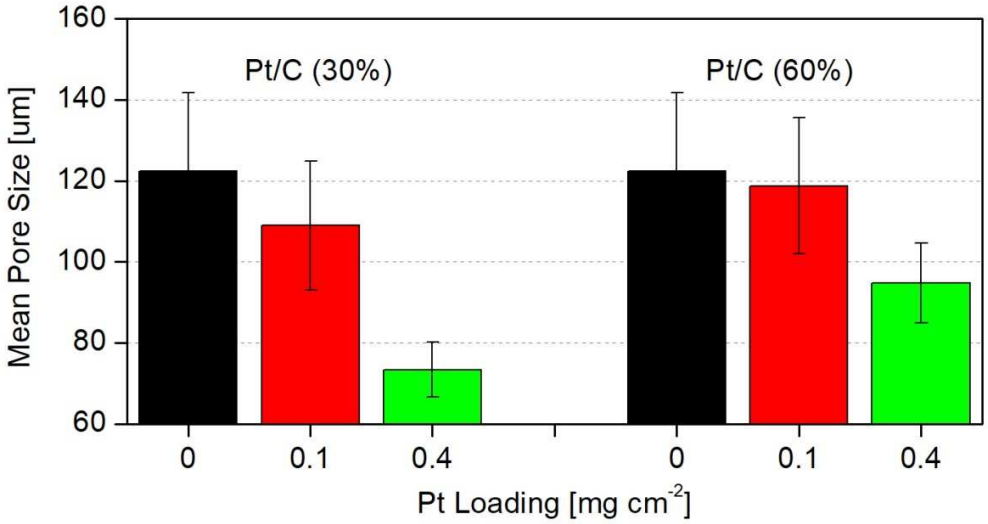

Fig. 5. Mean pore size of the porous electrodes with various Pt loadings and different types of catalysts.

3.6 Surface Fractal Dimension

Surface fractal dimension is a measure of the complexity of the porous structure. Normally, the Euclidean or topological dimension of a surface equals 2; however, the fractal dimension of the porous media, that is, D as defined in Eq. (14), can take a non-integer dimension between 2 and 3, and its value rises with the surface complexity or roughness [39,54]. When the fractal surface area is determined at different scale levels using various methods (e.g., gas adsorption [55], liquid extrusion [56], method of standard porosimetry [49,50,57], etc.), the fractal dimension can be calculated by fitting the data of the surface areas at different scale levels to Eq. (14). The value of *k* is a measure of the shape of the solid elements, which is formed during the fabrication or formation of the porous materials, while *D* is the fractal dimension which is a quantitative measure of the solid element distribution in space.

Table 1 presents the fractal dimension and the corresponding constant (or shape factor of the solid element) calculated through curve fitting. The pore surface area is a function of fractal dimension, *D,* and the constant, *k*. Using the least square curve fitting method as implemented in MATLAB's *lsqcurvefit* function [58], the experimental data on surface area distribution are fitted to Eq. (14), and the values of the fractal dimension, *D,* and the constant, *k* are obtained for the best fit. As can be seen, the surface fractal dimensions of the uncatalyzed and catalyzed electrodes are within the range of 2.7-2.9. As the Pt loading is increased, the fractal dimension and shape factor increase. This indicates that the surface properties and pore structure of the porous media become more complicated due to the addition of more Pt, carbon, and ionomer. Similarly, when the catalyst is changed to 60% Pt/C, the fractal dimension, D, and the shape constant, k, are smaller in comparison with 30% Pt/C. This is because less carbon and ionomer are sprayed on the GDL when the Pt loading is constant and less carbon and ionomer means that

the pore structure is less affected than that of 30% Pt/C. Therefore, fractal dimension is a good indicator of the complexity of the pore structure of the electrodes.

Table 1. Fractal dimension of the uncatalyzed and catalyzed electrodes.

Pt Loading [mg.cm^{-2}]	GDL	GDL+CL (30% Pt/C)		GDL+CL (60% Pt/C)	
	0	0.1	0.4	0.1	0.4
D	2.709	2.716	2.877	2.715	2.818
k [$\times 10^6$]	0.95	1.1	1.9	1.0	1.5
R^2 (coefficient of correlation)	0.9890	0.9724	0.9967	0.9750	0.9889

4. Conclusions

In this study, the effect of the catalyst layer (CL) on the pore structure of the electrode in polymer electrolyte membrane (PEM) fuel cells has been investigated by using the method of standard porosimetry (MSP). The catalyst inks are prepared from two different catalysts (30% and 60% Pt/C) and spray-deposited onto the gas diffusion layers (GDLs) for the Pt loadings of 0.1 and 0.4 mg·cm^{-2}. It is observed that the presence of the CL is of great significance to the overall pore structure of the electrode. As the Pt loading is increased, the electrode porosity decreases. Specifically, for 30% Pt/C, the electrode porosity decreases from 75% of the uncatalyzed GDL to 65%; and for 60% Pt/C, the porosity is reduced to 69%. It is also seen that the pores smaller than 100 nm in all the catalyzed electrodes increase with the Pt loading in comparison with the uncatalyzed one. These pores significantly contribute to the formation of the specific pore surface area (SSA) such that 95.0-96.5% of the cumulative pore surface area is

taken up by the pores smaller than 100 nm. For the constant Pt loading, the electrode made of a lower Pt/C ratio yields a thicker electrode, lower porosity, larger SSA, and smaller mean pore size. The surface fractal dimension of the electrode, between 2.709 and 2.877, is found to increase either with increasing Pt loading or decreasing Pt/C ratio, indicating more complex structure resulted from the fabrication of the CL on the electrode. Overall, this study highlights the importance of the CLs, hence its design parameters, i.e., Pt loading and Pt/C ratio, on the pore structure of the entire electrode in PEM fuel cells.

Acknowledgements

This work has received financial support from the Ontario-China Research and Innovation Fund (OCRIF Round 3), the Natural Sciences and Engineering Research Council of Canada (NSERC) via a Discovery Grant, and was conducted as a part of the Catalysis Research for Polymer Electrolyte Fuel Cells (CaRPE-FC) Network administered from Simon Fraser University and supported by Automotive Partnership Canada (APC) Grant No. APCPJ 417858 - 11 through the Natural Sciences and Engineering Research Council of Canada (NSERC).

References

[1] Yang P, Zhang H. Parametric analysis of an irreversible proton exchange membrane fuel cell/absorption refrigerator hybrid system. Energy 2015;85:458–67. doi:10.1016/j.energy.2015.03.104.

[2] Ramiar A, Mahmoudi AH, Esmaili Q, Abdollahzadeh M. Influence of cathode flow pulsation on performance of proton exchange membrane fuel cell with interdigitated gas distributors. Energy 2016;94:206–17. doi:10.1016/j.energy.2015.10.110.

[3] Yang S, Chellali R, Lu X, Li L, Bo C. Modeling and optimization for proton exchange membrane fuel cell stack using aging and challenging P systems based optimization

algorithm. Energy 2016;109:569–77. doi:10.1016/j.energy.2016.04.093.

[4] Chen B, Wang J, Yang T, Cai Y, Zhang C, Chan SH, et al. Carbon corrosion and performance degradation mechanism in a proton exchange membrane fuel cell with dead-ended anode and cathode. Energy 2016;106:54–62. doi:10.1016/j.energy.2016.03.045.

[5] Mirzaei F, Parnian MJ, Rowshanzamir S. Durability investigation and performance study of hydrothermal synthesized platinum-multi walled carbon nanotube nanocomposite catalyst for proton exchange membrane fuel cell. Energy 2017;138:696–705. doi:10.1016/j.energy.2017.07.098.

[6] Chavan SL, Talange DB. Modeling and performance evaluation of PEM fuel cell by controlling its input parameters. Energy 2017;138:437–45. doi:10.1016/j.energy.2017.07.070.

[7] Xu Q, Zhang W, Zhao J, Xing L, Ma Q, Xu L, et al. Effect of air supply on the performance of an active direct methanol fuel cell (DMFC) fed with neat methanol. Int J Green Energy 2018:1–8. doi:10.1080/15435075.2018.1431547.

[8] Qin Y, Du Q, Fan M, Chang Y, Yin Y. Study on the operating pressure effect on the performance of a proton exchange membrane fuel cell power system. Energy Convers Manag 2017;142:357–65. doi:10.1016/j.enconman.2017.03.035.

[9] Hong P, Xu L, Li J, Ouyang M. Modeling of membrane electrode assembly of PEM fuel cell to analyze voltage losses inside. Energy 2017;139:277–88. doi:10.1016/j.energy.2017.07.163.

[10] Taner T. Energy and exergy analyze of PEM fuel cell: A case study of modeling and simulations. Energy 2018;143:284–94. doi:10.1016/j.energy.2017.10.102.

[11] Huang Z-M, Su A, Liu Y-C. Hydrogen generator system using Ru catalyst for PEMFC

(proton exchange membrane fuel cell) applications. Energy 2013;51:230–6. doi:10.1016/j.energy.2013.01.020.

[12] Abdin Z, Webb CJ, Gray EMA. PEM fuel cell model and simulation in Matlab–Simulink based on physical parameters. Energy 2016;116:1131–44. doi:10.1016/j.energy.2016.10.033.

[13] Rahgoshay SM, Ranjbar AA, Ramiar A, Alizadeh E. Thermal investigation of a PEM fuel cell with cooling flow field. Energy 2017;134:61–73. doi:10.1016/j.energy.2017.05.151.

[14] Li X. Principles of Fuel Cells. New York: Taylor & Francis Group; 2006.

[15] Vol'fkovich YM, Sosenkin VE, Nikol'skaya NF, Kulova TL. Porous structure and hydrophilic-hydrophobic properties of gas diffusion layers of the electrodes in proton-exchange membrane fuel cells. Russ J Electrochem 2008;44:278–85. doi:10.1134/S102319350803004X.

[16] Shojaeefard MH, Molaeimanesh GR, Nazemian M, Moqaddari MR. A review on microstructure reconstruction of PEM fuel cells porous electrodes for pore scale simulation. Int J Hydrogen Energy 2016;41:20276–93. doi:10.1016/j.ijhydene.2016.08.179.

[17] Rahnavard A, Rowshanzamir S, Parnian MJ, Amirkhanlou GR. The effect of sulfonated poly (ether ether ketone) as the electrode ionomer for self-humidifying nanocomposite proton exchange membrane fuel cells. Energy 2015;82:746–57. doi:10.1016/j.energy.2015.01.086.

[18] Shahgaldi S, Zhao J, Alaefour I, Li X. Investigation of catalytic vs reactant transport effect of catalyst layers on proton exchange membrane fuel cell performance. Fuel 2017;208:321–8. doi:10.1016/j.fuel.2017.07.035.

[19] Zhao J, Shahgaldi S, Alaefour I, Yang S, Li X. Pore structure and effective diffusion coefficient of catalyzed electrodes in polymer electrolyte membrane fuel cells. Int J Hydrogen Energy 2018. doi:10.1016/j.ijhydene.2018.01.019.

[20] Kong IM, Jung A, Kim YS, Kim MS. Numerical investigation on double gas diffusion backing layer functionalized on water removal in a proton exchange membrane fuel cell. Energy 2017;120:478–87. doi:10.1016/j.energy.2016.11.100.

[21] Zamel N, Li X. Effective transport properties for polymer electrolyte membrane fuel cells - With a focus on the gas diffusion layer. Prog Energy Combust Sci 2013;39:111–46.

[22] Shen J, Zhou J, Astrath NGC, Navessin T, Liu ZS, Lei C, et al. Measurement of effective gas diffusion coefficients of catalyst layers of PEM fuel cells with a Loschmidt diffusion cell. J Power Sources 2011;196:674–8.

[23] Zamel N, Li X, Shen J. Correlation for the effective gas diffusion coefficient in carbon paper diffusion media. Energy and Fuels 2009;23:6070–8.

[24] Ozden A, Shahgaldi S, Zhao J, Li X, Hamdullahpur F. Assessment of graphene as an alternative microporous layer material for proton exchange membrane fuel cells. Fuel 2018;215:726–34. doi:10.1016/j.fuel.2017.11.109.

[25] Rouquerol J, Avnir D, Fairbridge CW, Everett DH, Haynes JH, Pernicone N, et al. Recommendations for the characterization of porous solid. Pure Appl Chem 1994;66:1739–58.

[26] Dullien FAL. Porous media: fluid transport and pore structure. New York: Academic Press; 1979.

[27] Jianzhong W, Huiping T, Jilei Z, Qingbo A, Hao Z, Jun M. Relationship between Compressive Strength and Fractal Dimension of Pore Structure. Rare Met Mater Eng

2013;42:2433–6. doi:10.1016/S1875-5372(14)60033-3.

[28] Farin D, Avnir D. Reactive fractal surfaces. J Phys Chem 1987;91:5517–21. doi:10.1021/j100306a001.

[29] Ye S, Vijh AK, Dao LH. Fractal dimension of platinum particles dispersed in highly porous carbonized polyacrylonitrile microcellular foam. J Electrochem Soc 1997;144:1734–8.

[30] Chen Y, Shen C, Lu P, Huang Y. Role of pore structure on liquid flow behaviors in porous media characterized by fractal geometry. Chem Eng Process Process Intensif 2015;87:75–80. doi:10.1016/j.cep.2014.11.014.

[31] Pitchumani R, Ramakrishnan B. A fractal geometry model for evaluating permeabilities of porous preforms used in liquid composite molding. Int J Heat Mass Transf 1999;42:2219–32. doi:10.1016/S0017-9310(98)00261-0.

[32] Shi Y, Xiao J, Pan M, Yuan R. A fractal permeability model for the gas diffusion layer of PEM fuel cells. J Power Sources 2006;160:277–83. doi:10.1016/j.jpowsour.2006.01.032.

[33] Zhang L-Z. A fractal model for gas permeation through porous membranes. Int J Heat Mass Transf 2008;51:5288–95. doi:10.1016/j.ijheatmasstransfer.2008.03.008.

[34] Cai J, Yu B, Zou M, Mei M. Fractal analysis of invasion depth of extraneous fluids in porous media. Chem Eng Sci 2010;65:5178–86. doi:10.1016/j.ces.2010.06.013.

[35] CAI J, YU B. Prediction of Maximum Pore Size of Porous Media Based on Fractal Geometry. Fractals 2010;18:417–23. doi:10.1142/S0218348X10005123.

[36] Pérez Bernal JL, Bello MA. Fractal geometry and mercury porosimetry - Comparison and application of proposed models on building stones. Appl Surf Sci 2001;185:99–107. doi:10.1016/S0169-4332(01)00649-3.

[37] Pfeifer P, Avnir D. Chemistry in noninteger dimensions between two and three. I. Fractal theory of heterogeneous surfaces. J Chem Phys 1983;79:3558–65. doi:10.1063/1.446210.

[38] Bhattacharya S, Gubbins KE. Fast method for computing pore size distributions of model materials. Langmuir 2006;22:7726–31. doi:10.1021/la052651k.

[39] Zeng Q, Luo M, Pang X, Li L, Li K. Surface fractal dimension: An indicator to characterize the microstructure of cement-based porous materials. Appl Surf Sci 2013;282:302–7. doi:10.1016/j.apsusc.2013.05.123.

[40] Farin D, Avnir D. The Reaction Dimension in Catalysis on Dispersed Metals. J Am Chem Soc 1988;110:2039–45. doi:10.1021/ja00215a004.

[41] Avnir D, Farin D, Pfeifer P. Chemistry in noninteger dimensions between two and three. II. Fractal surfaces of adsorbents. J Chem Phys 1983;79:3566–71. doi:10.1063/1.446211.

[42] Roohparvarzadeh S. Experimental Characterization of the Compressive Behaviour of Gas Diffusion Layers in PEM Fuel Cells. 2014.

[43] Xie J, More KL, Zawodzinski TA, Smith WH. Porosimetry of MEAs Made by “Thin Film Decal” Method and Its Effect on Performance of PEFCs. J Electrochem Soc 2004;151:A1841. doi:10.1149/1.1796991.

[44] Lobato J, Cañizares P, Rodrigo MA, Ruiz-López C, Linares JJ. Influence of the Teflon loading in the gas diffusion layer of PBI-based PEM fuel cells. J Appl Electrochem 2008;38:793–802. doi:10.1007/s10800-008-9512-8.

[45] Ito H, Heo Y, Ishida M, Nakano A, Someya S, Munakata T. Application of a self-supporting microporous layer to gas diffusion layers of proton exchange membrane fuel cells. J Power Sources 2017;342:393–404. doi:10.1016/j.jpowsour.2016.12.064.

[46] Oh H, Park J, Min K, Lee E, Jyoung JY. Effects of pore size gradient in the substrate of a

gas diffusion layer on the performance of a proton exchange membrane fuel cell. Appl Energy 2015;149:186–93. doi:10.1016/j.apenergy.2015.03.072.

[47] Yu Z, Carter RN, Zhang J. Measurements of pore size distribution, porosity, effective oxygen diffusivity, and tortuosity of PEM fuel cell electrodes. Fuel Cells 2012;12:557–65. doi:10.1002/fuce.201200017.

[48] Volfkovich YM, Sosenkin VE, Bagotsky VS. Structural and wetting properties of fuel cell components. J Power Sources 2010;195:5429–41. doi:10.1016/j.jpowsour.2010.03.002.

[49] Volfkovich YM, Sakars AV, Volinsky A a. Application of the standard porosimetry method for nanomaterials. Int J Nanotechnol 2005;2:292–302.

[50] Volfkovich YM, Bagotzky VS. The method of standard porosimetry. 1. Principles and possibilities. J Power Sources 1994;48:327–38.

[51] Morrow NR, Harris CC. Capillary Equilibrium in Porous Materials. Soc Pet Eng J 1965;5:15–24.

[52] Nimmo JR. Porosity and pore size distribution. Encycl Soils Environ 2004:295–303. doi:10.1016/B978-0-12-409548-9.05265-9.

[53] Zhao J, Shahgaldi S, Alaefour I, Xu Q, Li X. Gas permeability of catalyzed electrodes in polymer electrolyte membrane fuel cells. Appl Energy 2018;209:203–10. doi:10.1016/j.apenergy.2017.10.087.

[54] Shelberg MC, Lam N, Moellering H. Measuring the Fractal Dimensions of Surfaces. Proc Sixth Int Symp Comput Cartogr Auto-Carto 1983;6:319–28.

[55] Yan Z, Chen C, Fan P, Wang M. Pore Structure Characterization of Ten Typical Rocks in China. Electron J Geotech Eng 2015;20:479–94.

[56] Miller B, Tyomkin I. An Extended Range Liquid Extrusion Method for Determining Pore

Size Distributions. Text Res J 1986;56:35–40.

[57] Volfkovich YM, Bagotzky VS. The method of standard porosimetry 2. Investigation of the formation of porous structures. J Power Sources 1994;48:339–48.

[58] Pant LM, Mitra SK, Secanell M. Absolute permeability and Knudsen diffusivity measurements in PEMFC gas diffusion layers and micro porous layers. J Power Sources 2012;206:153–60.

Highlights:

- Studied the effect of Pt loading and catalyst type on electrode pore structure
- Characterized electrode pore structure by the Method of Standard Porosimetry
- Quantified porosity, pore size, pore surface area, and surface fractal dimension
- Observed 95.0-96.5% of surface area contributed by small pores (<100 nm)
- Quantified the surface fractal dimension of electrode within the range of 2.7-2.9